Impact of finite laser bandwidth on the critical dimension of L/S structures

Peter De Bisschop
IMEC
Kapeldreef 75
B-3001 Leuven, Belgium
E-mail: bisschop@imec.be

Ivan Lalovic
Fedor Trintchouk
Cymer Inc.
17075 Thornmint Ct.
San Diego, California 92127

Abstract. We investigate the effect of finite laser bandwidth on line-space (L/S) imaging, both through simulations and experiment. We will show that the primary effect of laser bandwidth is a change of the optical-proximity behavior of the scanner, i.e., a modification of the critical dimensional pitch [CD(Pitch)] characteristic, and that depth of focus typically remains unaffected. The simulation part of this study resulted in a simple estimator, expressing bandwidth-induced CD changes in terms of the "quadratic focus-sensitivity" ($\equiv 1/2\ d^2CD/dF^2$) of the L/S structure, a parameter which we call the "second moment" of the laser spectrum, M_2, and the longitudinal chromatic-aberration of the scanner ($dF/d\lambda$) only. The experimental part of this study, in which we measured CD(pitch) curves at different laser-bandwidth settings of the ASML XT:1700i NA =1.20 immersion scanner at Interuniversitary Micro-Electronic Centre (IMEC), confirms the results of the theoretical part, while relating the bandwidth dependency of the CD effects also to the experimentally available E95 metric. We conclude that even though the laser bandwidth of modern scanners is quite low, bandwidth effects do contribute to their proximity behavior and impact proximity stability as well as scanner-to-scanner proximity differences. We present a critical evaluation of current laser-bandwidth metrics and comment on the trade-off between the average laser bandwidth and laser bandwidth stability in order to achieve a required level of proximity control (e.g., between scanners). [DOI: 10.1117/1.2964297]

Subject terms: laser bandwidth; optical proximity; optical lithography; second moment; E95; E99.

Paper 07090R received Dec. 2, 2007; revised manuscript received Apr. 1, 2008; accepted for publication Apr. 14, 2008; published online Aug. 13, 2008.

1 Introduction

Several studies of the effect of finite laser bandwidth on the critical dimensional (CD) of line-space (L/S) structures have been published in the past,[1–8] and the basic effect is well known. Even though laser wavelength (and, hence, bandwidth) affects several lens aberrations, by far the major effect is the formation of separate best-focus planes by each of the wavelengths in the laser spectrum, leading to a net focus blur in the resulting image. The projection-lens dependency of this effect is described by the longitudinal chromatic-aberration constant, defined as

$$F_\lambda \equiv \frac{dF}{d\lambda} \quad \text{units:}[\mu\text{m/pm}]. \tag{1}$$

The value of this lens constant is different for every lens type, but typically ranges in the 0.2–0.5 μm/pm range[6]. Throughout this paper, we will use the F_λ value of the ASML XT:1700i NA=1.20 immersion scanner, though we cannot explicitly state its value in this paper because of confidentiality reasons.

Lithographic simulations are usually done under the assumption that the illuminator is monochromatic, but when the value of F_λ is known, finite-laser bandwidth simulations can, in principle, be done by sampling the actual laser spectrum by a finite set of individual wavelengths, λ_j, and then making an incoherent superposition of the image intensities of each of the contributing wavelengths. The image formed by wavelength λ_i is calculated as the image at a defocus $\Delta F_j = F_\lambda\ (\lambda_j - \lambda_0)$, where (in this paper) we define λ_0 to be the wavelength where the maximum laser intensity occurs. This procedure is represented in Eq. (2) and illustrated in Fig. 1. If $I_{1\lambda}(F)$ is the image intensity at defocus F calculated in the monochromatic case, then the finite-bandwidth image intensity, corresponding to the laser spectrum S, which we will write as I_S, becomes

$$I_S = \frac{\int d\Delta\lambda\ S(\Delta\lambda)\ I_{1\lambda}(\lambda)}{\int d\Delta\lambda\ S(\Delta\lambda)} \approx \frac{\sum_j S(\Delta\lambda_j) I_{1\lambda}(\lambda_j)}{\sum_j S(\Delta\lambda_j)} \equiv \frac{\sum_j S_F(\Delta F_j) I_{1\lambda}(F_j)}{\sum_j S_F(\Delta F_j)}. \tag{2}$$

$S(\Delta\lambda)$ is the laser spectrum (i.e., the relative intensity versus wavelength), with $\Delta\lambda_j = (\lambda_j - \lambda_0)$. The second part of Eq. (2) rewrites the superposition in terms of defocused images, putting $\Delta F_j = F_\lambda \Delta\lambda_j$, and "converting" the laser

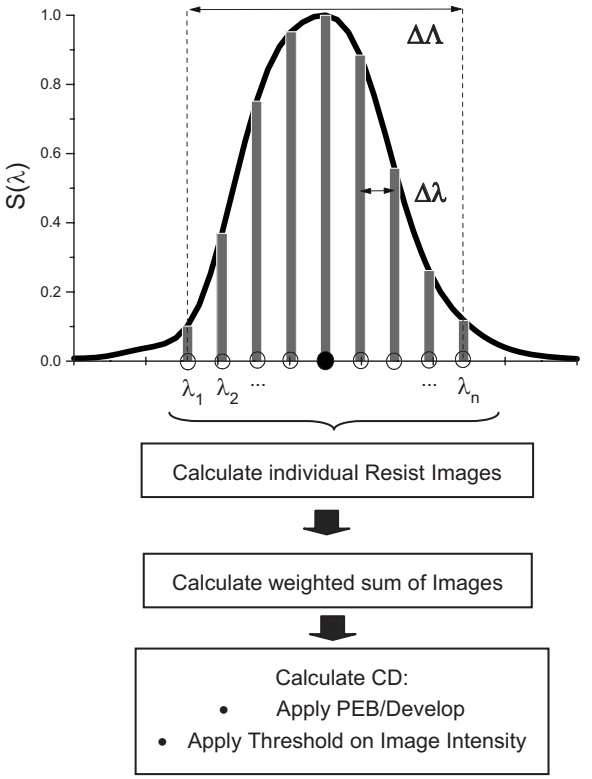

Fig. 1 Representation of a finite-bandwidth CD calculation: the image intensity is calculated as a weighted sum of monochromatic images for a finite wavelength sampling over the laser spectrum. $\Delta\Lambda$ and $\Delta\lambda$ stand for the total width of the sampling interval and the sampling distance, respectively (see Sec. 2.2).

Table 1 List of less common symbols and quantities used in this paper.

Quantity	Unit	Meaning	Definition
F_λ	μm/pm	Longitudinal chromatic lens aberration	$dF/d\lambda$
Q_F	μm/μm^2	Quadratic focus sensitivity of litho structure	$\frac{1}{2}d^2CD/dF^2$
$S(\lambda)$		Laser spectrum (i.e., intensity versus wavelength)	
M_2	pm^2	Second moment of laser spectrum $S(\lambda)$	Eq. (8)
m_2	pm^2	We use small caps if the quantity referred to is the result of a proportionality fit between ΔCD and Q_F, as given in Eq. (7) or (12), and not calculated from a laser spectrum S directly.	Eq. (7) or (12)
E95	pm	Wavelength interval containing 95% of the energy	Ref. 2
E99	pm	Wavelength interval containing 99% of the energy	Similar to E95

spectrum S into defocus units (i.e., $S(\Delta\lambda)\Delta\lambda \equiv S_F(\Delta F)\Delta F$). (Note that the sum approximations of the original integral expression assume a simple uniform sampling plan. More efficient calculation of the integral can also be done by some suitable "quadrature" integration, in which case appropriate weight factors w_j would have to be added in the sum terms of Eq. (2).

In case one wants to do only the "resist-image" calculations,[9] $I_{1\lambda}$ and I_S are 1-D intensity functions, and CDs are obtained by applying an intensity threshold. In the case of full-resist model (FRM) simulations, $I_{1\lambda}$ and I_S describe the (2-D) image intensity within the entire resist layer, and CDs are obtained by applying a resist model.

Simulations of the type of Eq. (2) have been done before, though usually in the simple resist-image approach (i.e., not using a FRM). Also, no study has yet been published in which the effect of bandwidth was studied in a systematic way, including, e.g., dependencies on L/S type, illumination mode or changes in the laser spectrum. This paper is an attempt to fill this gap. On the basis of such a more systematic simulation study (Sec. 2), we will first come up with a simple "estimator" or "law" that describes the bandwidth-induced CD effects in terms of simple metrics that represent the lens, the laser spectrum, and the defocus-behavior of the litho structure. Then (Sec. 3), we report on an experiment in which we verified the results of the simulation work, an experiment in which we measured CD(pitch) curves on the XT:1700i NA=1.20 immersion scanner at Interuniversitary Micro-Electronic Centre (IMEC), under different settings of the laser bandwidth. Finally, in Secs. 4 and 5, we try to convert the findings of this paper into practical conclusions concerning laser-bandwidth metrics and comment on the relation between the laser-bandwidth requirements and the optical proximity effect (OPE) budget of the scanner. The reader, who does not want to go through all the technical details of this paper but is only interested in its practical conclusions can skip Secs. 2 and 3 and can go to Secs. 4 and 5 immediately. Throughout the paper, we will be using a number of quantities and symbols that would be less known to the general reader. Table 1 summarizes these.

2 Simulation Study of the Laser-Bandwidth Effect

2.1 *Laser Spectra*

Simulations of finite-bandwidth effects reported in the literature are sometimes being done assuming a certain functional shape for the laser spectrum, $S(\lambda)$, like a Gaussian, Lorenzian, or "modified Lorentzian"[5] function, but it is preferable to use measured laser spectra, which has also been done before.[1–3,5,8] (Ref. 8, in particular, discusses the differences between the approximations and measured spectra.) Although analytical functions resemble actually

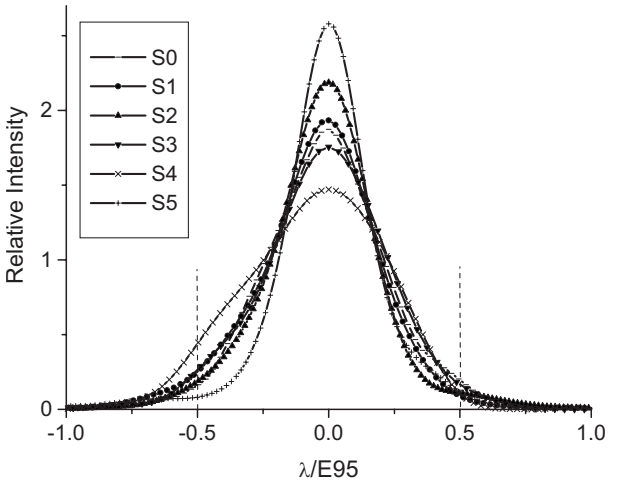

Fig. 2 Six laser spectra used in the simulation part of this study. The horizontal wavelength scale is normalized by dividing it with the E95 value of each of the spectra to better show the shape differences between the spectra.

measured laser spectra quite well in the higher-intensity part of the spectrum, they do not necessarily match the tails of measured spectra very well, and as a consequence, the through-pitch/through-focus CD differences for the best Gaussian and modified Lorentzian analytical fits to the measured data is several nanometers.[8] The reason is, as we shall demonstrate later on in this section, that these tails play an essential role in the magnitude of the bandwidth effect; thus, in the current study we have always used spectra that were measured at Cymer on actual 193 nm excimer lasers.

We put together a set of six spectra that differ from each other in shape and width. The shape and width were intentionally varied using nonstandard operating modes to cover a very broad range of conditions, which should exceed what can be expected on production lasers, but it is important to note that all spectra used still meet the bandwidth spec of current hyper-NA scanners (i.e., E95 smaller than some maximum value, e.g., 0.5 pm). Figure 2 shows the spectra used in the simulation part of this work. Doing simulations for different spectral shapes will help ensure that the conclusions of our work are not too dependent on the particular spectrum that was used. Table 2 shows the E95 values for each of these six spectra. (A definition of the E95 metric can be found in Ref. 2.)

Table 2 Six laser spectra used in our simulation study. The metrics E99 and M_2 will be defined further on in this paper. M_2 was calculated with a 29 points sum formula [see Eq. (8)].

Spectrum Label	E95 (pm)	E99 (pm)	M_2 (pm^2)
*S*0	0.27	0.468	0.00448
*S*1	0.233	0.360	0.0036
*S*2	0.378	0.593	0.00765
*S*3	0.160	0.224	0.00169
*S*4	0.218	0.285	0.00357
*S*5	0.327	0.522	0.00523

2.2 *Laser Spectrum Sampling*

First, we will look into the question how we should best do the spectrum sampling when doing a finite-bandwidth image calculation [type Eq. (2)], i.e., how many wavelengths should we include and where should we place them? The goal is to find a trade-off between accuracy and calculation time: including more wavelengths is, in principle, more accurate but also unrealistically pushes the calculation time.

We will look into this sampling question in two steps, trying to establish a reasonable choice for

1. $\Delta\Lambda$=the total width of the sampling interval
2. $\Delta\lambda$=the distance between the sampling points

(For the time being, we will assume evenly spaced sampling points, which, in fact, is not necessarily the optimum scenario.) The two quantities $\Delta\Lambda$ and $\Delta\lambda$, are illustrated in Fig. 1.

We used two sampling schemes to determine reasonable settings for $\Delta\Lambda$ and $\Delta\lambda$:

1. Using very small values for $\Delta\lambda$, start probing the spectrum from its maximum (λ_0) onward, gradually adding more wavelengths at either side of the maximum, thus gradually increasing the total sampling width $\Delta\Lambda$
2. For a given total sampling width $\Delta\Lambda$, and starting from a fine sampling distance $\Delta\lambda$, gradually increase $\Delta\lambda$, thus gradually decreasing the number of wavelengths used to sample $\Delta\Lambda$.

In both cases, we calculate the bandwidth-induced CD change for a number of L/S structures and look for an economic sampling scheme that still gives a result that is close to the CD result obtained with the most extensive sampling case, which we take as the actual bandwidth effect. Of course, the optimum that will come out will depend on the accuracy one wishes to obtain, and in that sense, it is subjective. But we do the exercise for several pitches and for our six laser spectra to be at least more or less independent to these two "variables."

For simplicity, we have done the calculations of this section by extracting CDs using a fixed threshold on 1-D resist images. Rather than the absolute CD values, we are interested in the CD change with respect to the monochromatic case, i.e.,

$$\Delta CD_S(\Delta\Lambda,\Delta\lambda) \equiv CD_S(\Delta\Lambda,\Delta\lambda) - CD_0, \tag{3}$$

CD_0 and CD_S being the monochromatic and finite-bandwidth CD respectively, for a given spectrum $S(\lambda)$ and sampling parameters $\Delta\Lambda$ and $\Delta\lambda$. (Note: the mask line width for each of these pitches was taken such that all L/S structures print at 50 nm for a common resist-image threshold.)

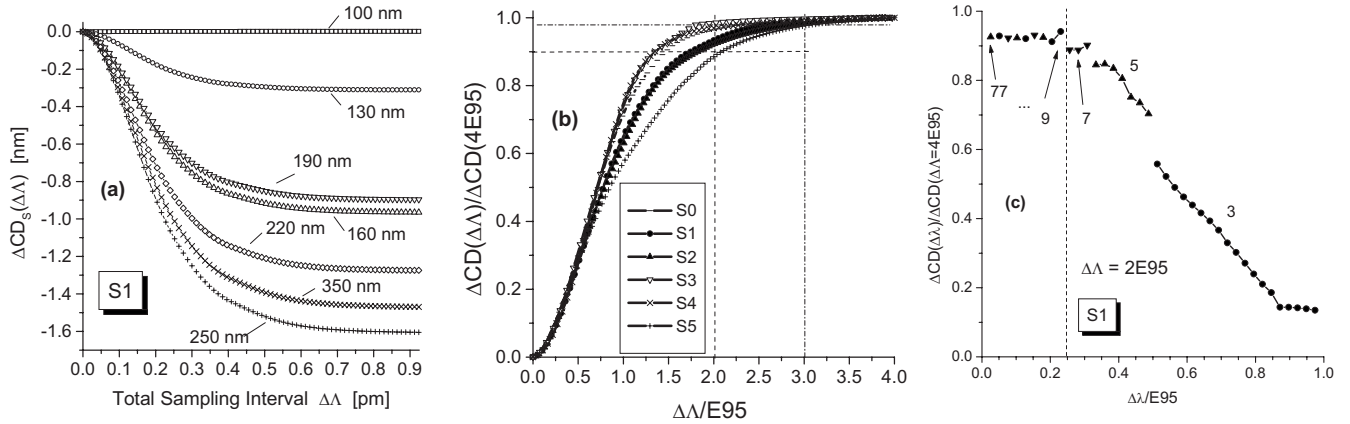

Fig. 3 Simulation of bandwidth-induced CD changes, ΔCD_S, using different spectrum-sampling conditions (NA=1.20 cQuad20 σ=0.96/0.60 *XY*-polarized, MoSi mask, resist-image calculation with Solid-E, image convolution with off-line software). (a) Sampling scheme 1, with $\Delta\lambda$ =fixed at 0.006 pm. Calculated is $\Delta CD_S(P)$ versus $\Delta\Lambda$ for seven different pitches P (value of pitch indicated in plot). (b) Rescaled version of (a) with averaging over all pitches [vertical scale rescaled according to Eq. (4)]. Shown are the results obtained with all six laser spectra of Fig. 2. (c) Sampling scheme 2, with $\Delta\Lambda \approx 2E95$. The numbers next to the data points indicate how many sampling wavelengths were used in the calculation (numbers between 9 and 73 not indicated in the plot). Example of spectrum *S*0; the other spectra show similar results.

The results of this exercise are shown in Fig. 3. Figure 3(a) first of all shows the calculated ΔCD-results versus $\Delta\Lambda$, for each of the seven pitches included in the calculation. Obviously ΔCD_S is different for all pitches, which is easy to understand: denser L/S structures have a weak CD-(focus) dependency and will be less sensitive to the bandwidth effect, which consists of a convolution of images over defocus, than semidense or isolated structures that have a stronger CD(focus) dependency. However, in all cases we find that $\Delta CD_S(\Delta\Lambda)$ saturates at the high $\Delta\Lambda$-end of the curve. If we rescale all $\Delta CD_S(\Delta\Lambda, P)$ curves by dividing them by $\Delta CD_S^{max}(P)$ (i.e., their value at $\Delta\Lambda = \Delta\Lambda_{max}$), thus showing the relative bandwidth effect for a given value of $\Delta\Lambda_{max}$, we find that these rescaled curves are identical for all L/S structures included (i.e., the rescaled curves are pitch independent). Figure 3(b) shows the resulting rescaled curves, averaged over all pitches P,

$$\Delta CD_S^{rel}(\Delta\Lambda) \equiv \text{Mean}_P\left\{\frac{\Delta CD_S(\Delta\Lambda, P)}{\Delta CD_S^{max}(P)}\right\} \quad (4)$$

in which we now have also scaled the horizontal axis by expressing $\Delta\Lambda$ in units of E95, and where we have repeated the calculation for the six laser spectra of Fig. 2.

Although there is an obvious dependency of $\Delta CD_S^{rel}(\Delta\Lambda)$ on the actual spectral shape, it is also clear that the sampling interval should be somewhere between 2E95 and 3E95 to capture ~90 to 100% of the bandwidth effect, whereas a sampling interval of E95 would only capture ~60% of the total effect. This underlines the importance of including the tails of the spectrum into the calculations, which can be easily understood: even though the tails of the spectrum only carry low intensity, they contribute to the image convolution of Eq. (2) with "far"-out-of-focus images.

For the remainder of this section, we will use a sampling interval $\Delta\Lambda$=2E95, which "captures" >~90% of the bandwidth effect for the six spectra we consider. It must be remarked, however, that the correctness of this statement is somewhat dependent on the accuracy with which the far-tail intensity of the spectrum is known. For $\Delta\lambda$>E95, the intensity of our experimental spectra becomes <0.1% of the peak intensity, and an accurate measurement of such low intensities requires very careful background subtraction and detector deconvolution. A detailed discussion of these topics, though very interesting and in fact important, is beyond the scope of the current paper, and we will assume here that considering a sampling interval $\Delta\Lambda$=2E95 is sufficient indeed. Useful to note is that, again for the six spectra considered, this 2E95 interval contains ~99% of the total energy in the spectra. In Table 2, we have added the values of a E99 metric of each spectrum. E99 has a similar definition as E95: it is the width of the interval containing 99% of the total spectrum intensity. With respect to the bandwidth effect on $\Delta CD_S^{rel}(\Delta\Lambda)$, Fig. 3(b) tells us that E99 should more completely describe the bandwidth effect on CD compared to E95.

Figure 3(c) shows the result of the second sampling type: we now fixed $\Delta\Lambda$=2E95 and vary $\Delta\lambda$ from very small to large, thus also decreasing the number of sampling wavelengths used. Again we found that rescaling ΔCD_S by its maximum value removes the pitch dependency in our results; thus, we only consider the pitch-averaged curve for each of the six spectra. Also here, we express the horizontal scale in units of E95. Reading the graphs of Fig. 3(c) from right to left, we see that three and five sampling points seem insufficient for capturing >90% of the bandwidth effect, but a sampling with seven or nine wavelengths seems sufficient. The corresponding sampling distance is $\Delta\lambda \approx$E95/4. Thus, the conclusion of this section is that we do not need to include very many sampling wavelengths into a finite-bandwidth calculation to achieve fairly accurate results.

By considering a clever nonuniform sampling scheme, it is likely that the number of required samples could be further reduced, probably to five or seven. In the remainder of this section, we will however continue to use the simple uniform-sampling approach.

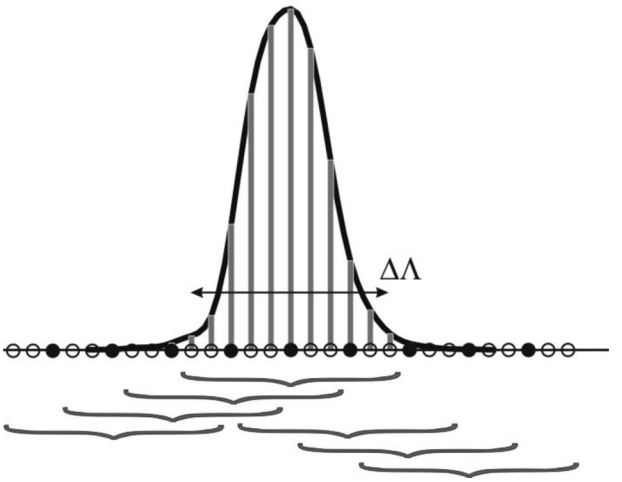

Fig. 4 Illustration of how the finite-bandwidth images at several defocus positions (black dots) were calculated by superimposing saved resist-images at a finer spacing (black and open dots). A resist model is then applied to the convoluted images.

Table 3 Illumination mode and pitch ranges used (6% attenuated PSM MoSi mask). cQuad20 has four pie-shaped poles with a 20 deg opening angle, placed on the *X*- or *Y*-axis. DipoleX35 has two pie-shaped poles with a 35 deg opening angle, placed on the *X*-axis. Quasar35 has four pie-shaped poles with a 35 deg opening angle, placed on the diagonal between the *X*- and *Y*-axes.

Label	Pitches included (nm)	Illumination $\sigma_{outer}/\sigma_{inner}$	Source polarization
Annular1	95–400	Annular σ=0.96/0.80	*XY* polarized
cQuad	95–400	cQuad20 σ=0.96/0.80	*XY* polarized
DX	95–400	DipoleX35 σ=0.96/0.80	*Y* polarized
Annular2	135–400	Annular σ=0.96/0.80	*XY* polarized
Quasar	135–400	Quasar35 σ=0.96/0.80	Unpolarized

2.3 *Bandwidth-Induced CD Changes Calculated with Full-Resist Model (FRM)*

2.3.1 *Simulation cases and conditions*

We will now report a more systematic simulation of bandwidth-induced effects, investigating the effect through pitch, for several illumination modes and for the six laser spectra of Fig. 2. We will not only consider the effect in best focus, but calculate through focus (to look for possible effects on depth of focus), and we will use a full-resist model, not to be affected by the simplifications which the threshold-on-resist-image approach might invoke.

Because of the volume of the simulation work and the fact that full-resist simulations are more time consuming than threshold-on-resist-image-type calculations, we improved the efficiency of our calculation approach in the following way (see also Fig. 4). The 2-D image intensity in resist was first calculated at a set of defocus values, with a focus spacing ΔF, which was consistent with the desired $\Delta\lambda$ sampling (i.e., $\Delta F = F_\lambda \Delta\lambda$), and all these images were separately saved. Then, the finite-bandwidth CD for a given defocus value F was calculated by superimposing the saved images at a set of n defocus values F_j around F according to Eq. (2), the values of measured spectrum S being interpolated at the selected F_j positions.

With this approach, all images only need to be calculated once and can then be reused for combining them into the finite-bandwidth images at the different defocus positions of interest, and also the calculation can easily be repeated for a different laser spectrum, as this only calls for a different weighting in the convolution of the "monochromatic" images. As such an approach could not be done with the commercial simulators we had at our disposal,[10] we collaborated with the group of Andreas Erdmann of the IISB Fraunhofer Institute in Erlangen, Germany: their internal simulator, Dr.Litho 0.5, was setup to achieve the required intermediate image saving, image convolution, and application of the resist model to the convoluted (i.e., finite-bandwidth) images.

According to the results of Sec. 2.2, we made sure that in all cases the sampling covered a 2E95 interval (also for the largest E95 of the six spectra), and that the sampling distance was not larger than E95/4 (also for the smallest E95), which led us to a 29-sampling point scheme. (Note that we need a 29 point sampling only because we wanted to simultaneously accommodate six different spectra.)

Table 3 illustrates the illumination settings and pitch ranges we used in the calculations. These settings are relatively arbitrary but were chosen to represent a reasonably wide range of conditions at NA=1.20 L/S printing. For each illumination mode, the dose to size was calculated for the smallest pitch (in the monochromatic case), and the mask line width for the other pitches was biased to print to 45 nm at the same dose. We used an identical dose for the finite-bandwidth and monochromatic calculations.

2.3.2 *Quantities calculated*

We calculated CD(Focus) curves both in the monochromatic (1λ) and the finite-bandwidth [$S(\lambda)$] case. Such a CD versus focus curve can usually be fitted quite well by a parabola,

$$\mathrm{CD}(F) = \mathrm{CD}_0 + Q_F(F - F_0)^2. \tag{5}$$

All calculated curves are actually well fitted by this simple parabolic function, which implies that we can look for the effect of finite bandwidth on the three fit-parameters

1. CD_0: CD at "Best Focus" F_0 [being taken here as the top of the CD(F) curve]. This is the quantity that corresponds to the OPE effect.
2. F_0: position of this Best Focus.
3. Q_F: "quadratic focus dependency" of the L/S structure ($=1/2\ d^2\mathrm{CD}/dF^2$; expressed in microns per microns squared).

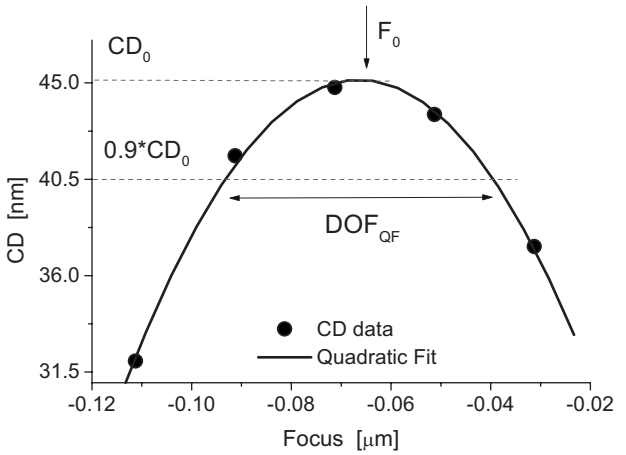

Fig. 5 Illustration of the quadratic fit of a CD(Focus) curve, and the meaning of the Q_F factor.

Especially, this quadratic focus dependency, or Q_F factor, will turn out to be very useful in the quantification of the bandwidth effect, as we shall see further on; thus, it is useful to consider it in a little more detail.

$Q_F \approx 0$ means that the CD(F) behavior is almost isofocal and, hence, that the depth-of-focus (DOF) will be large. A large value of $|Q_F|$ implies a small DOF. Although there is no formula linking Q_F directly to the DOF as it is usually defined, we can "convert" the fitted value of Q_F into a DOF-like quantity (which we write as $\mathrm{DOF_{QF}}$), using the following definition (see also Fig. 5):

$$\mathrm{DOF_{QF}} \equiv 2\sqrt{\frac{\mathrm{CD_0}/10}{|Q_F|}}. \tag{6}$$

$\mathrm{DOF_{QF}}$ is the focus interval for which CD(F) stays within 10% from the value at best focus, F_0. If $|Q_F|$ is too large, then this focus interval will be "unmanufacturably" small. An example can give us a feel for the order of magnitude. Assume that $\mathrm{CD_0}=45$ nm and that we require $\mathrm{DOF_{QF}} \geq \sim 100$ nm, then it follows that we require $|Q_F| \leq \sim 1.8\ \mu\mathrm{m}/\mu\mathrm{m}^2$.

2.4 *Simulation Results, Comparing Finite-Bandwidth to Monochromatic Case*

2.4.1 *Optical proximity effect,* $\Delta\mathrm{CD_0}(P)$

$\Delta\mathrm{CD_0}$ corresponds to the CD difference between the finite-bandwidth CD and monochromatic CD, calculated in best focus, and is similar to the quantity defined in Eq. (3) (i.e., $\Delta\mathrm{CD_0} \equiv \mathrm{CD_0}(S) - \mathrm{CD_0}(\text{monochromatic})$, S again representing the selected laser spectrum).

We have calculated this quantity for the six laser spectra of Table 2 and the five Illumination-mode cases of Table 3 (and their corresponding pitches). Figure 6 shows an

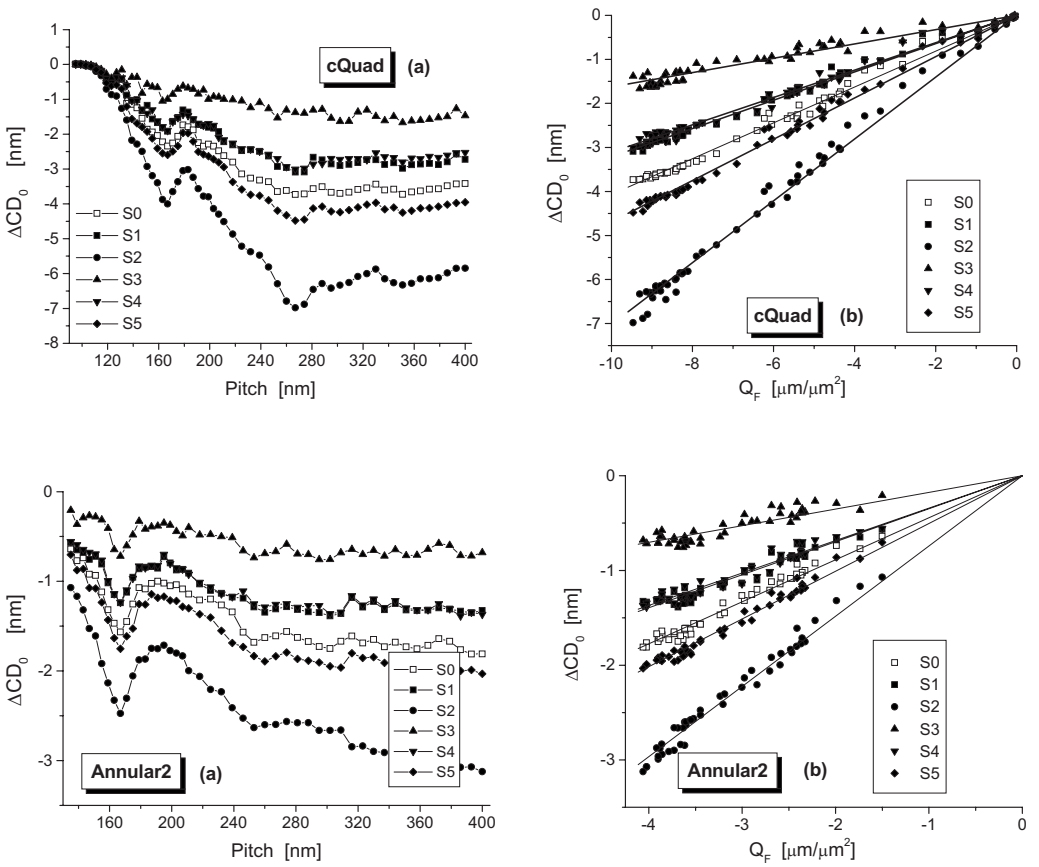

Fig. 6 Calculated values of finite-bandwidth–monochromatic CD differences, $\Delta\mathrm{CD_0}(P)$, for the six laser spectra of this study, plotted versus pitch as well as versus $Q_F(P)$. Examples for the cQuad and one of the Annular2 settings of Table 3, calculated with the FRM.

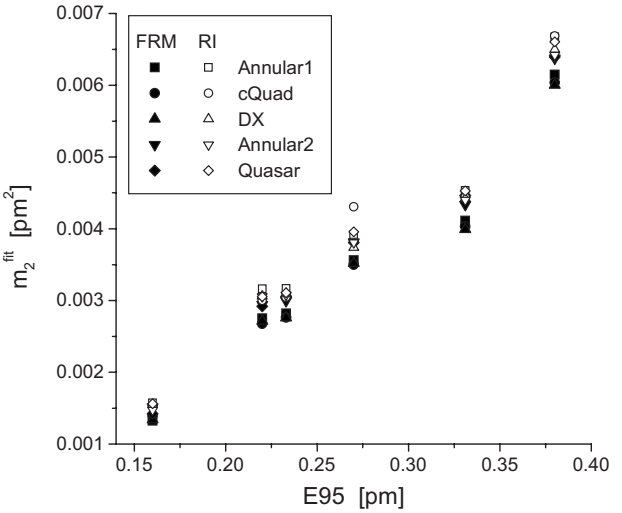

Fig. 7 Values of the fitted proportionality factor m_2^{fit}, for the five illumination settings of Table 3, calculated both with the FRM (closed symbols) and with a simple threshold-on-resist-image model (open symbols).

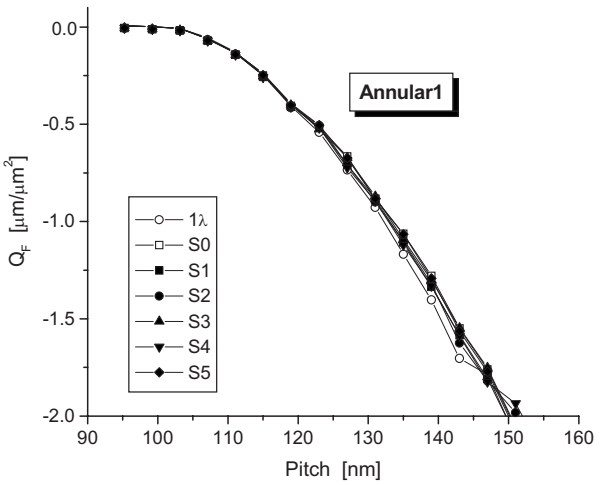

Fig. 8 Calculated value of Q_F for the case of monochromatic illumination (labeled 1λ) and for the six laser spectra of this study. For the "manufacturable" (unassisted) *L/S* structures ($|Q_F| \leq 2\ \mu m/\mu m^2$) laser bandwidth does not affect Q_F (cases of annular1 illumination).

example of the result we obtained, for the case of the cQuad illumination and one of the Annular cases. Figure 6(a) plots the calculated ΔCD_0 data versus the pitch of the L/S structures. The bandwidth effect is clearly dependent on the pitch, confirming that finite-bandwidth contributes to the optical proximity behavior of the scanner, and hence, to scanner-to-scanner proximity differences (if the scanners have different laser spectra or different models of scanner which may have different levels of chromatic aberrations).

Figure 6(b) replots the same data but now using the Q_F factor for each of the L/S structures on the horizontal scale. It is immediately clear that the second plot reveals proportionality between ΔCD_0 and Q_F, which we write as (the reason why it is convenient to introduce F_λ^2 into the proportionality between ΔCD_0 and Q_F will become apparent in Sec. 2.5)

$$\Delta CD_0(P) \equiv m_2^{fit}(S) F_\lambda^2 Q_F(P) \quad [m_2^{fit}] = pm^2. \tag{7}$$

For now, the proportionality factor m_2^{fit} is a mere fit parameter only. It obviously must depend on the laser spectrum *S*, but at this point the exact relationship is still unknown. (We will however propose an equation expressing the relation between m_2^{fit} and *S* in Sec. 2.5). Interestingly, m_2^{fit} is found to be largely independent of the illumination mode: to within 10%, we find identical values of m_2^{fit}, and also, when repeating the same simulations with the simpler threshold-on-resist-image approach (for the same cases), we find values for m_2^{fit} that are quite close to the FRM values. This can be seen in Fig. 7, where the values of m_2^{fit}, for the six laser spectra and the five illumination modes are plotted, both calculated with the FRM and the threshold-on-resist-image mode. This observation suggests that m_2^{fit} depends primarily on the details of the laser spectrum itself, but is virtually independent of the L/S structure and illumination mode. We will show that this is indeed the case in Sec. 2.5. In Fig. 7, we plot m_2^{fit} versus E95 and see that these two parameters seem to be correlated, but this relationship is not yet clear at this point (but we return to this argument in Secs. 2.5 and 3.2).

A practical note with respect to the magnitude of the ΔCD_0 values shown in Fig. 6, is that we must remind that structures with large $|Q_F|$ values ($> \sim 2\ \mu m/\mu m^2$) would not occur in actual designs. Large-pitch L/S structures would normally have assist features to increase their DOF and decrease $|Q_F|$, hence also decreasing ΔCD_0. Thus, the ΔCD_0 values in Fig. 6 are overestimating the to-be-expected OPE effect in realistic cases. Also, we are often not so much concerned with finite bandwidth versus monochromatic CD differences, but rather with CD difference that correspond to different laser spectra. We will return to this argument in Sec. 4.

2.4.2 *Through-focus behavior*

It is interesting to also investigate a possible bandwidth effect on the fit parameters F_0 and Q_F of Eq. (6), i.e., investigate whether the finite-bandwidth affects Best Focus and DOF.

Asymmetries in the shape of the laser spectrum (and these indeed do occur in all the measure spectra we are using in this study) do generate small best-focus shifts, but in the cases we calculated, these best-focus shifts are almost pitch independent and not larger than ~5 nm between different spectra. Therefore, these calculated best-focus effects have no practical consequences and can be further ignored.

Intuitively, one might expect that the finite-laser bandwidth would affect the value of Q_F and, hence, the DOF, but our simulations show that this is not the case, (except for structures with $|Q_F| > \sim 5\ \mu m/\mu m^2$). If, as we argued before, we assume that "manufacturable" structures must have $|Q_F| \leq \sim 2\ \mu m/\mu m^2$, we find no difference in the value of Q_F between monochromatic simulations and the finite-bandwidth cases of this study. Figure 8 illustrates our results for the case of one of the Annular settings, where we show only the simulation results for L/S structures with $|Q_F| \leq 2\ \mu m/\mu m^2$.

The conclusion is that the effect of finite laser bandwidth on the through-focus behavior of the L/S structures is negligible. It is however good to mention explicitly that this conclusion applies to the "normal" type of laser spectra only (i.e., spectra that conform with the max-E95 spec) and that our conclusions do not apply to special applications using, e.g., focus drilling, FLEX or RELAX, in which case DOF is affected. RELAX,[11] for example, uses a strongly modified laser spectrum (consisting of two peaks instead of one) and does therefore not fit into the class of spectra we are considering in the current study.

2.5 *Analytical Estimator for the Bandwidth-Induced OPE Effect*

In this section, we investigate whether and how we can relate the bandwidth-dependent proportionality factor, m_2^{fit}, of Eq. (7) to the actual spectrum $S(\lambda)$. In Sec. 2.4.1, we showed that the fitted value of m_2^{fit} is approximately the same in case of threshold-on-resist-image or full-resist model simulations. When making certain assumptions about the shape and focus dependency of the resist image, one can, in fact, derive an approximating analytical expression for m_2^{fit}.

What we find is that m_2^{fit} can be related to the laser spectrum by

$$m_2^{\text{fit}}(S) \approx M_2(S) \equiv \frac{\int_{-\infty}^{+\infty} d\lambda \lambda^2 S(\lambda)}{\int_{-\infty}^{+\infty} d\lambda S(\lambda)} \approx \frac{\sum_j \lambda_j^2 S(\lambda_j)}{\sum_j S(\lambda_j)}, \tag{8}$$

in which we call M_2 the second moment of the laser spectrum S. (Note that this quantity is similar to the rms metric in Ref. 6.) Equations (7) and (8) can then be combined into

$$\Delta \text{CD}_0(P) \approx F_\lambda^2 M_2(S) Q_F(P) \tag{9}$$

[ΔCD_0 represents for the CD difference between a monochromatic illumination and an illumination with a spectral distribution S, but one can easily rewrite Eq. (9) to represent the CD difference between two different spectral distributions, S_1 and S_2, by replacing the M_2 term at the right-hand side by $\Delta M_2 \equiv M_2(S_1) - M_2(S_2)$.] The proof of this equation, as well as the assumptions made to derive it, is given in the Appendix. Although Eq. (9) is really an approximate formula, our work (including the experimental part in Sec. 3) indicates that it is actually sufficiently accurate for most practical purposes.

We tested the validity of Eq. (9) on the simulated data of this section by verifying the correlation between the fitted m_2^{fit} values (see Fig. 7) and M_2 as calculated from the spectrum S using Eq. (8), in which we replaced the integral by a sum over the sampling wavelengths we used in the simulation (recall that we actually did a 29-wavelength sampling in our simulations). The result of this correlation is shown in Fig. 9 and confirms that Eq. (8) is a reasonable approximation. (If m_2^{fit} is exactly equal to M_2, the slope of the correlation plot in Fig. 9 should be 1. This is however not the case. In the Appendix, we show that this is largely due to the fact that the Q_F value we use in the fit of Eq. (7) was obtained from a parabolic fit representation of the CD(F) dependency [see Eq. (5)], whereas it is more accurate to fit CD(F) with a fourth- or even sixth-order polynomial. If we use such a more accurate formula, then the m_2^{fit} to M_2 correlation slope increases to values between 0.93 and 0.99, as can be seen in Fig. 18 in the Appendix.)

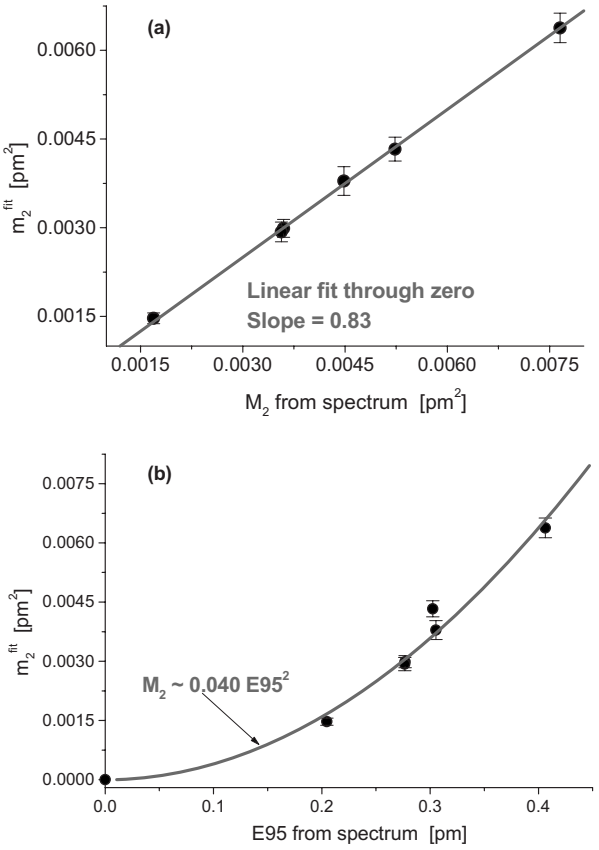

Fig. 9 (a) Correlation plot between the fit parameter m_2^{fit} and M_2 calculated with Eq. (8) (applied to the 29-point sampled spectra of this study), supporting the validity of Eq. (8). (An improved correlation is shown in Fig. 17 in the Appendix.) (b) correlation plot between the fit parameter m_2^{fit} and the E95 value (calculated from the 29-point sampled spectra of this study). These data are consistent with a quadratic dependency, $m_2^{\text{fit}} \sim \text{E95}^2$.

Equation (9) is attractively convenient; it expresses the finite-bandwidth effect as a product of a factor that depends on the lens design only (F_λ^2), one that depends on the through-focus behavior of the L/S structure only (Q_F) and one that depends on the laser spectrum only (M_2). Note that also a change in illumination mode or resist process would be entirely incorporated in Q_F. A major inconveniency of this expression, however, is that, in general, M_2 is unknown. Onboard laser metrology does not measure this quantity, the traditional bandwidth metric being E95. Also when the laser spectrum is measured on an external spectrometer, as was the case for the six spectra used in this study, the calculation of M_2 is problematic. The occurrence of the λ^2 factor in its definition, see Eq. (8), easily leads to a diverging integral, unless the intensity in the tails of $S(\lambda)$ is sufficiently small. Accurate measurements of these tails impose severe demands on the dynamic range and background subtraction of the $S(\lambda)$ measurement, demands that

are not easy to meet. (Note that we did not have that problem when calculating M_2 for the correlation in Fig. 9: as we did the simulations with a limited set of sampling wavelengths, we created cases where the spectrum tails do not extend beyond the 29 sampling wavelengths, and therefore, the calculation of M_2 poses no problem.)

From a practical point of view, it would be more practical to have an Eq. (9)–type expression that would relate the bandwidth effect to E95, rather than M_2, as E95 is readily available from the onboard laser metrology. The theory, however, does not offer such an equivalent equation. If one assumes an analytic functional expression for $S(\lambda)$, such as a Gauss or a (modified) Lorentz function, one can, in principle, derive a functional relationship between E95 and M_2, but the result one obtains depends on the function that was selected, and for some functions of S, the M_2 integral even diverges. Nevertheless, both a Gauss and a modified Lorentz[5] lead to a quadratic dependency between E95 and M_2. Equation (10) gives an expression[12] for M_2 in case of a modified Lorentz function, S_{ML},

$$S_{\mathrm{ML}}(\lambda) = \frac{1}{(2\lambda/\Delta)^{\eta} + 1}$$

$$\Rightarrow M_2 = \frac{\Delta^2}{4} \frac{\sin(\pi/\eta)}{\sin(3\pi/\eta)} \quad \text{if } \eta > 3$$

η being a positive, real value. (10)

For $\eta \leq 3$, M_2 diverges. Δ is equal to the full width at half maximum (FWHM) of the spectrum. As E95 is proportional to the FWHM, Eq. (10) tells us that $M_2 \propto \mathrm{E95}^2$. However, because the M_2 to Δ (and hence also the M_2 to E95) proportionality factor depends on the shape-factor η, as Eq. (10) clearly shows, it is obvious that there is no fixed ratio between M_2 and $\mathrm{E95}^2$ that applies to all spectral shapes.

Nevertheless, we can look what the relationship between M_2 and E95 of the spectra we used in this section looks like. Figure 9 (bottom graph) shows that the M_2 (E95) dependency following from our simulations is consistent with such a quadratic proportionality, though the data would not exclude another dependency. We will come back to this issue in Sec. 3, when analyzing experimental bandwidth-induced ΔCD data. Also, there we will find that, although there is no *a priori* proof for an $\mathrm{E95}^2$ law, the data do not disagree with such a dependency.

3 Experimental Verification of the Laser-Bandwidth Effect

3.1 *Goal and Design of the Experiment*

The results of the simulations done in this study [see, e.g., Eq. (9)] tell us that the lithostructure dependency in the expression of the bandwidth-induced CD changes is given by the quadratic focus sensitivity factor, Q_F. This Q_F factor not only covers the structure dependency, but also the illumination-mode and resist-process dependency. This is a practically useful finding, because Q_F can be easily determined from a measured or simulated CD(focus) curve. Another conclusion of the simulations was that the OPE effect is, in fact, the only effect of the finite laser bandwidth: we, for example, do not expect any sizable effect on the DOF of the lithostructure for the range of bandwidths we consider in this work.

Table 4 Conditions used in the bandwidth-detuning experiment.

Bandwidth-setting		NA=1.20, cQuad20 σ=0.96/0.60 *XY* polarized Pitches: 100–400 nm		NA=1.20, Annular σ=0.96/0.70 *XY* polarized Pitches: 110–400 nm	
Label	E95 (pm)	E_{ref} (mJ/cm^2)	F_{ref} (μm)	E_{ref} (mJ/cm^2)	F_{ref} (μm)
S_{E1}	0.222	23.75	−0.086	22.7	−0.112
S_{E2}	0.309	23.82	−0.082	23	−0.113
S_{E3}	0.381	23.85	−0.095	23.05	−0.117
S_{E4}	0.41	23.9	−0.094	22.9	−0.107
S_{E5}	0.480	23.82	−0.07	22.72	−0.106

All these results can be verified experimentally, if one could compare experimental CD(focus) curves for, e.g., different bandwidth settings on one and the same scanner. For the scanner we used in our experiment, bandwidth adjustment is not readily available to the scanner user from the laser or scanner software. However, for this system, Cymer developed experimental techniques to adjust the laser bandwidth by varying the laser operating conditions over a range of bandwidth settings. (In future systems, bandwidth tuning will become more accessible to the scanner user by software-controlled Tunable ABS, advanced bandwidth stabilization, module in Cymer lasers.)

We therefore did an experiment in which we measured the CD(focus) behavior for a set of ~30 L/S structures, using five laser-bandwidth conditions and two illumination modes (i.e., 10 combinations in total). Table 4 summarizes the conditions we used for this experiment.

All wafers were exposed on the ASML XT:1700i NA =1.20 immersion scanner at IMEC (resist process: 120 nm TarF-Pi6-001-me on 95 nm ARC29SR). We exposed focus-exposure matrix wafers and measured the Bossung curve of the selected L/S structures, i.e., the CD(F,E) in resist, using scatterometry. The measured Bossung data were then fitted and from the fit we interpolated the CD value at a chosen "reference" focus and dose: CD(P,E_{ref},F_{ref}). Figure 10 shows an example. E_{ref} and F_{ref} were determined separately for each wafer of the experiment but are, of course, the same for all L/S pitches measured from the same wafer. For F_{ref}, which stands for "best focus," we took the maximum of the CD(E_{ref},F) curve of the most isolated pitches used in the experiment. E_{ref} was taken as the dose to size of the most iso-focal pitch. We evaluated the CD-differences between the different wafers (i.e., bandwidth conditions) for a given illumination mode then as

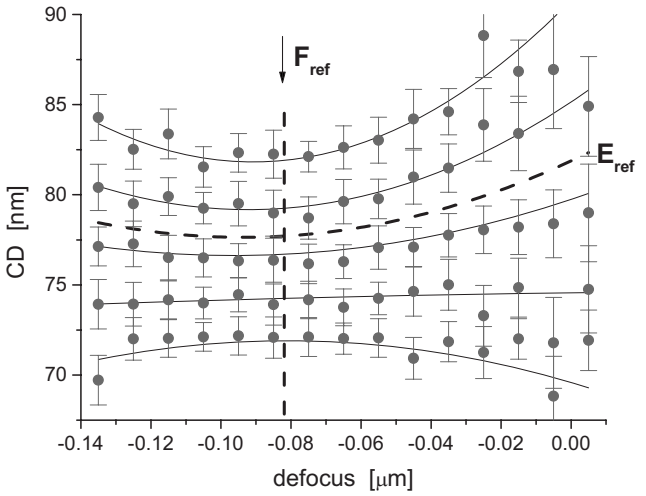

Fig. 10 Example of a measured (symbols) and fitted (lines) Bossung for one of the L/S structures of the experiment, and the interpolation of $\mathrm{CD}(P, E_{\mathrm{ref}}, F_{\mathrm{ref}})$ from the fit.

$$\Delta\mathrm{CD}_{\mathrm{SE}j}(P) \equiv \mathrm{CD}_{\mathrm{SE}j}(P) - \mathrm{CD}_{\mathrm{SE1}}(P), \tag{11}$$

where we, arbitrarily, took bandwidth-setting S_{E1} (the one with the lowest value of E95) as the reference for our data analysis (i.e., the setting to which we compare the results from the other settings). The experimental procedure used ensures that $\Delta\mathrm{CD}_{\mathrm{SE}j}$ will be 0 for the most iso-focal pitch (which we have used to set the value of E_{ref}). From each of the fitted $\mathrm{CD}(P, E_{\mathrm{ref}}, F)$ curves, we can also easily determine the value of Q_F.

3.2 *Experimental Results*

We first examine the experimental results for Q_F. Figure 11 shows the results for the cQuad20 illumination case. As expected from the simulations (see, e.g., Fig. 8), we find no significant bandwidth dependency of Q_F within the experimental error: down to $|Q_F| \sim 2\ \mu\mathrm{m}/\mu\mathrm{m}^2$ all curves are virtually identical. At lower Q_F values, the measured differences seem to be somewhat outside the estimated error bars, even though the behavior of the data in this region still suggests that the differences are due to measurement noise alone. Anyway, structures with such a high value of $|Q_F|$ would not be manufacturable, so that a possible small bandwidth effect on DOF is of little practical relevance.

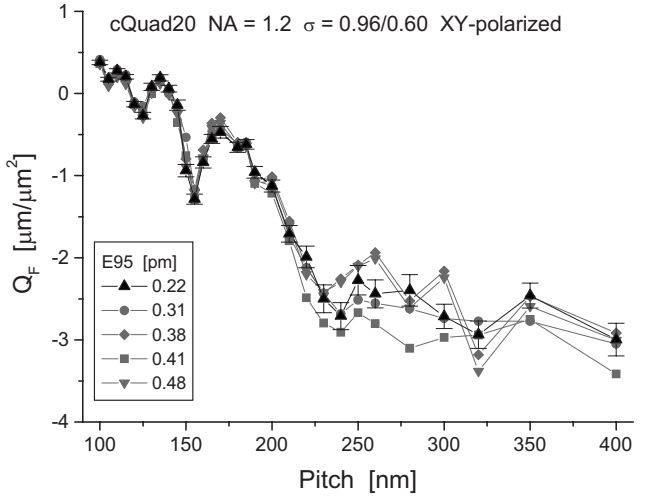

Fig. 11 Comparison of the $Q_F(P)$ results for the five bandwidth conditions of the experiment (evaluated for the cQuad20 illumination mode case). The error bars shown correspond to ± the "standard error" as defined in the "multiple regression" theory.[13] We only added error bars to one of the curves; the errors on the data of the other curves are comparable, but are not shown to maintain the readability of the plot.

From this observation it follows that we can evaluate a possible $\Delta\mathrm{CD}$-Q_F correlation using any of the measured $Q_F(P)$ curves, or an average over the five measured curves (for a given illumination mode). The result is shown in Fig. 12: even though each individual curve is relatively noisy, the linear correlation we deduced for the simulation is also confirmed by the experimental results.

To complete the comparison to the simulation results, we now only need to verify whether the correlation factors are the same for the two illumination modes. This is done in Fig. 13, where we plot the fitted values of the correlation factor, expressed as a quantity Δm_2, which is defined through the following equation:

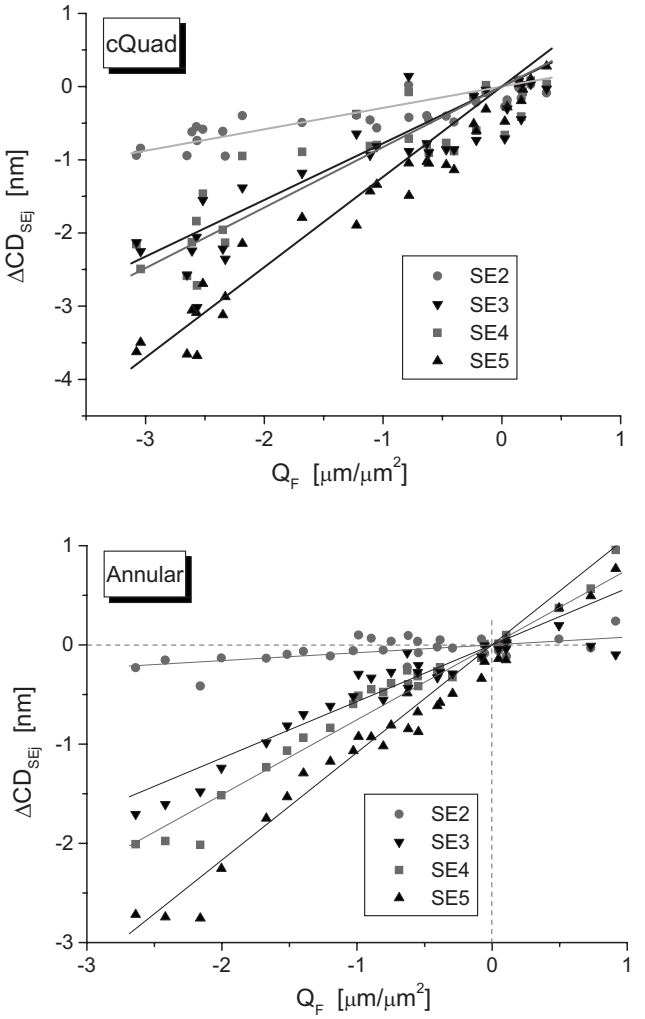

Fig. 12 $\Delta\mathrm{CD}$-Q_F correlation for the two illumination modes of the experiment.

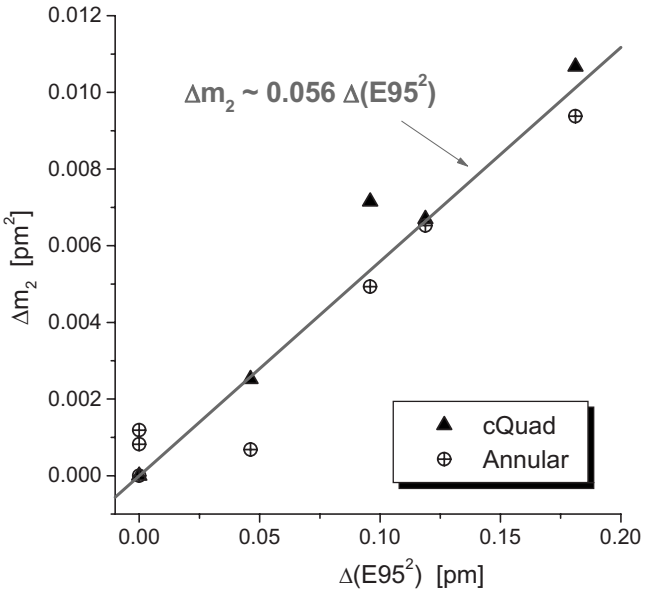

Fig. 13 Fitted values of Δm_2 versus $\Delta(\mathrm{E95}^2)$, showing that the results are indeed equal for the two illumination modes.

$$\Delta \mathrm{CD}_{S_{Ej}}(P) \equiv \Delta m_2(S_{Ej}) F_\lambda^2 Q_F(P). \tag{12}$$

This expression is a modified version of Eq. (7): Δm_2 is now a fit parameter that is derived from the experimental CD- and Q_F-data, and must, of course, be related to the difference between the laser spectra of setting S_{Ej} and S_{E1}. Unfortunately, we cannot compare these fitted Δm_2 values to second-moment data from the laser, because the second moment is not available from the laser self-metrology, and an external spectrometer was not available during the experiment to measure the laser spectra and deduce M_2 values from them. The only available bandwidth-related parameters obtained from the laser onboard metrology were the E95 and FWHM values. Therefore, we plot the fitted values of Δm_2 versus the $\Delta(\mathrm{E95}^2)$ $[\equiv \mathrm{E95}(S_{Ej})^2 - \mathrm{E95}(S_{\mathrm{E1}})^2]$ parameters (Fig. 13).

The first observation from Fig. 13 is that the fit parameters Δm_2 seem, within the accuracy of this experiment, indeed equal for the two illumination settings of the experiment. This is consistent with the results of the simulations, from which Δm_2 would only be a function of the laser-spectrum, and not depend on the illumination mode, nor on the L/S structure. Thus, even though several of the data curves in Figs. 12 and 13 are relatively noisy (we are measuring quite small effects), the overall agreement with the conclusions from the simulation part of our study is satisfactory.

The final question we address is whether the experiment can provide a quantitative relation between the fitted values of Δm_2 and the experimental E95 values. The reason for this is a practical one. As we have discussed previously, the second moment is not available from the laser self-metrology and due to the unavoidable noise in the spectrum tails, it is nontrivial to measure this parameter, which would make it difficult to realize such M_2 metrology. E95, on the other hand, is available and is currently the common bandwidth metric.

As we did in Sec. 2.5, we can try to relate Δm_2 to $\Delta(\mathrm{E95}^2)$, but we can equally try a relationship with ΔE95. In fact, our experimental data do not allow one to distinguish between these two (and possible other) possibilities. Fitting both options to the data yields

$$\Delta m_2 = m_Q \Delta(\mathrm{E95}^2) \quad \text{with} \quad m_Q \approx 0.056 \tag{13a}$$

or

$$\Delta m_2 = m_L \Delta(\mathrm{E95}) \quad \text{with} \quad m_L \approx 0.037 \text{ pm} \tag{13b}$$

with an approximately equal goodness of fit. Equation (13a) can be compared to a similar relationship we obtained from the simulated data, where we found a proportionality factor of 0.04, a value (though not equal) that is of the same order of magnitude as the 0.056 that we deduced from our experimental data. Thus, we can now take these dependencies and derive some practical conclusions with respect to acceptable bandwidth changes, if we make certain assumptions about the acceptable contribution to the OPE budget.

4 OPE Budget and Requirements on Bandwidth Control

The two previous sections concentrated on a fundamental study of the effects of finite laser bandwidth and resulted in a number of equations that can be used to quantify the effect on OPE, which we found to be the major effect. We now want to turn to the practical messages that follow from this work and make an estimate of how laser-bandwidth differences or changes contribute to OPE budgets or, alternatively, how a given OPE-budget requirement could be translated into a bandwidth requirement and bandwidth-stability requirement. We will do this for the simple case of 50 nm L/S imaging on a NA=1.20 immersion scanner, as this is closest to the conditions of our experiment. Our study suggests that the most appropriate laser-bandwidth metric that we could use is the second moment of the laser spectrum, M_2. However, this is not an available metric in the laser self-metrology, which is why we will use the E95 metric instead. Even though the theory we developed does not provide a direct link between bandwidth-induced CD changes and E95, we did demonstrate that both our simulation and experimental ΔCD data appear to be consistent with a $\Delta(\mathrm{E95}^2)$ dependency [see, e.g., Eqs. (12) and (13a)]. The arguments below could be easily restated in terms of M_2.

First, we assume that assist-feature rules have been found for all structures of interest, such that $|Q_F| \leq 1.8\ \mu\mathrm{m}/\mu\mathrm{m}^2$. Structures that do not meet this requirement have a too low DOF anyway, and would be classified as "forbidden." Then, the "allowed" structures that are most sensitive to laser bandwidth variations would be the ones with $|Q_F| \approx 1.8\ \mu\mathrm{m}/\mu\mathrm{m}^2$.

Next we must make an assumption about the variation of E95 values we can expect (due to variations over time or due to laser-to-laser differences). Let us consider a population of laser spectra with E95 values centered around an average value, $\mathrm{E95}_{\mathrm{av}}$, and with an E95 range, $\Delta E95$, around this mean value. The results of Sec. 3 then allow us to make

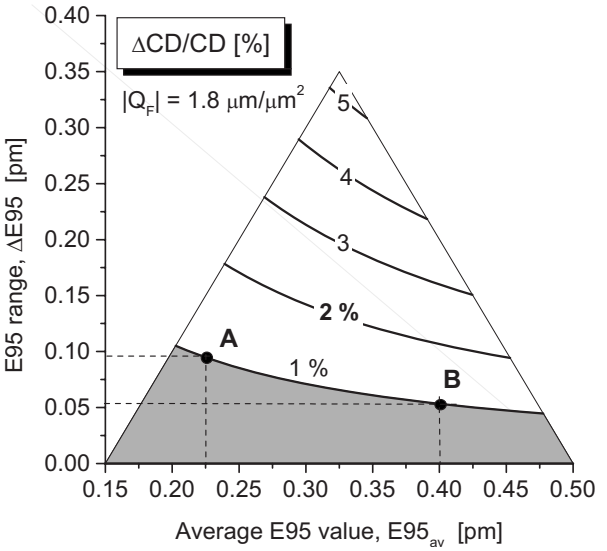

Fig. 14 Relative CD variations for a $|Q_F|=1.8\ \mu m/\mu m^2$ structure, as a function of the mean value and the range of the E95 distribution. The lines connect points of equal ΔCD/CD, the values being plotted on the lines. All points within the central triangular area have 0.15 pm < E95 < 0.5 pm. For making this particular graph, we used $F_\lambda=0.35\ \mu m/pm$, which is the average value of the 0.2–0.5 $\mu m/pm$ range that is stated as typical in Ref. 6.

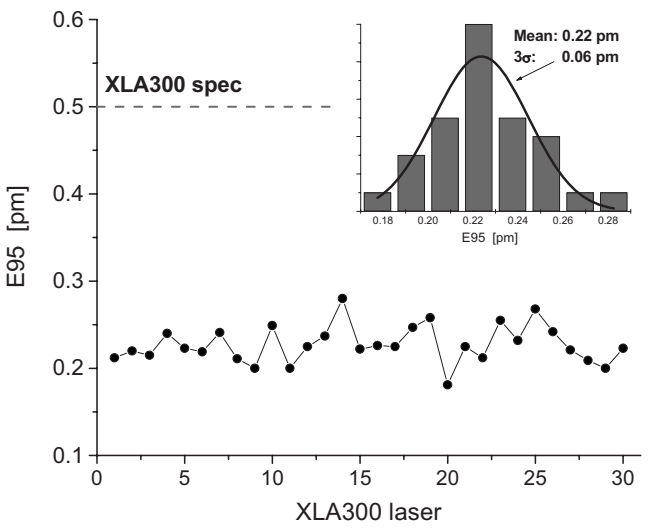

Fig. 15 Actual laser-to-laser E95 variation for a typical series of XLA300 lasers (not using ABS).

an estimate of the bandwidth-induced CD differences between the two extreme E95 settings within this range (i.e., $E95_{av} \pm \Delta E95/2$) as follows:

$$\Delta CD = F_\lambda^2\, Q_F\, \Delta M_2 \approx 0.056\, F_\lambda^2\, Q_F\, (E95_{max}^2 - E95_{min}^2)$$
$$= 0.056\, F_\lambda^2\, Q_F\, (2E95_{av}\Delta E95). \quad (14)$$

In this equation, ΔCD stands for the max-min CD difference between the two extremes from this laser population (i.e., the lasers characterized by $E95_{max}$ and $E95_{min}$). The bandwidth spec on the XT:1700i laser (i.e., the XLA300) is that E95 ≤ 0.5 pm, so $E95_{max}$ would then be 0.5 pm. E95 values close to zero are not expected to occur, so let's assume that the smallest E95 value that is likely to occur is $E95_{min}$=0.15 pm. Figure 14 plots the result we the obtain from Eq. (14), or rather it plots the relative CD variation, expressed in percent (i.e., 100 × ΔCD/CD), for CD =50 nm.

We can now use this plot to estimate acceptable E95-distribution parameters if we choose a maximum allowed ΔCD/CD. Say, for example, that we require that ΔCD/CD ≤ 1% (i.e., that we only are willing to allow 1% of the CD budget to bandwidth effects). All $(E95_{av}, \Delta E95)$ combinations in the gray-shaded area of Fig. 14 satisfy this requirement. It is clear that such a tight CD requirement does not necessarily imply that E95 must be extremely small, but rather that we need to impose a certain control over the allowed E95 variation around some average value. Points A and B on the ΔCD/CD=1% line illustrate this point. Point A corresponds to a quite small value of $E95_{av}$ of 0.225 pm, which permits a E95-range of ~0.1 pm. Point B, however, corresponds to a distribution of laser spectra with an average E95 that is much larger, namely, 0.4 pm, but if the E95-range around this value is ≤ ~0.05 pm, we still achieve the required ΔCD/CD ≤ 1%.

Equation (14) makes clear that we need to put an upper limit to $E95_{av} \times \Delta E95$ in order to control the optical proximity behavior within a group of scanners with a certain E95 distribution, rather than to the maximum value of E95 for the individual systems. In the latter scenario, and assuming that we accept E95 ≤ 0.5 pm as a sufficient requirement on the bandwidth, Fig. 14 shows that ΔCD/CD up to ~5% could occur (always for the most sensitive structures, i.e., structures with a large value of $|Q_F|$), a value that would certainly not be acceptable or would require some type of "proximity matching or tuning" on the scanners.

What, then, is the actual performance of current litho lasers? Figure 15 shows measured E95 values from a series of 30 XLA300 lasers. It is clear that the actual E95 variation is a lot smaller than the E95 < 0.5 pm specification allows. With a $E95_{av}$ of ~0.22 pm and a ΔE95 < 0.1 pm, we can read from Fig. 14 that the maximum OPE difference between these lasers would stay < ~1% indeed.

The actual trade-off between mean E95 and E95 stability is dependent on the specific imaging application, and active control of bandwidth (E95) stability, as well as tuning of the E95 mean, will be available on next-generation systems. Cymer has developed active bandwidth stabilization (ABS) and tunable ABS, which enable the user to optically control and modify the E95. The initial systems could, for example, feature an ABS set point of 0.3 pm with a ΔE95 of 0.1 pm over the life or a fleet of systems and over all operating conditions. Thus, the technical facilities to be compliant with a requirement on $E95_{av} \times \Delta E95$, as suggested by Eq. (14), are becoming available.

Finally, we can also use Eq. (14) to estimate the possible bandwidth-induced CD difference on a distribution of scanners that have an E95 variation of the type shown in Fig. 15, which do not yet feature active E95 compensation. We now also do not limit to the most focus-sensitive structures, but look at series of L/S structures through pitch, where

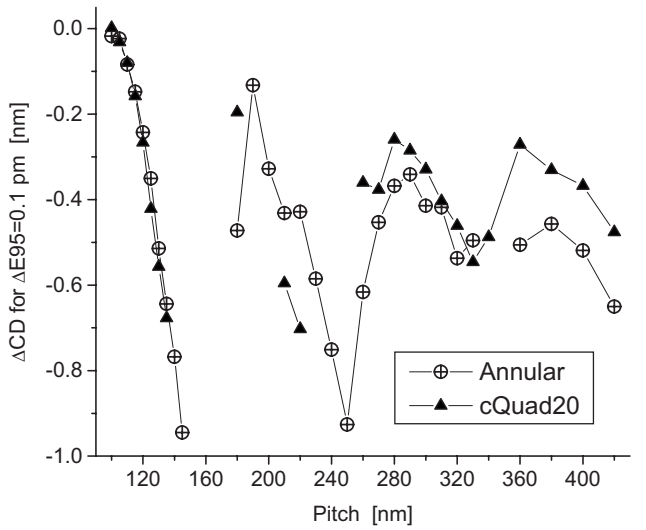

Fig. 16 Estimated ΔCD for *L*/*S* structures through pitch, with an appropriate assist-feature rule applied whenever possible, according to Eq. (14) and assuming an E95 distribution, as in Fig. 15, and exclude "forbidden pitches."

some appropriate assist-feature placement has been done to increase the DOF, but such that $|Q_F| < 1.8\ \mu\text{m}/\mu\text{m}^2$ for all structures. Figure 16 shows a typical result, for imaging L/S structures on a NA=1.20 scanner, with an on-wafer target CD of 50 nm. The OPE-differences do not exceed ~1 nm, which is an acceptable result.

5 Summary and Conclusions

We have investigated the effect of finite-laser bandwidth on simple L/S structures. The first part of this paper was devoted to a combined simulation and experimental fundamental study of the impact of finite laser bandwidth. The main conclusions of the technical part of this work can be summarized as follows:

1. Laser bandwidth contributes primarily to the OPE performance of the scanner, i.e., it induces CD changes (compared to the monochromatic illumination case), but has no significant effect on DOF nor on the position of best focus.
2. Accurate simulations of laser-bandwidth effects are usually done by superimposing monochromatic images. We showed that (when doing a uniform sampling over the laser spectrum) one needs to include at least seven to nine defocus positions, covering an interval of at least 2E95, in order to obtain the finite-bandwidth CD value in a single defocus position. This result emphasizes the importance of the tails of the laser spectrum.
3. Simulating finite-bandwidth effects requires detailed knowledge of the entire laser spectrum (information that is usually not available). We therefore tried to derive a simple estimator for bandwidth-induced CD effects that we can apply without requiring such detailed information nor lengthy calculations. The expression we derived (see Eq. (9)), shows that the quadratic focus sensitivity (a quantity which we call the Q_F factor) describes the structure, illumination mode, and resist-process dependency of the CD effects quite well. The dependency on the laser spectrum was shown to be given by the second moment of the spectrum, M_2 (a quantity that is currently not a readily available laser metric and is, in fact, not straightforwardly derived from measured laser spectra, because the inevitable measurement noise in the tails of measured spectra easily gives rise to a nonconverging result). Thus, with respect to suitable bandwidth metrics, our study puts M_2 forward as the most fundamental one, because it is the quantity that follows from the theoretical arguments we make in the Appendix. Our theory did not come up with any intrinsic link between the OPE effect and E95. However, both our simulated and measured CD data, were found to be compatible with a (more phenomenological) $E95^2$ bandwidth dependency [Eqs. (12) and (13)], showing that E95 does not have to be rejected as a practical bandwidth metric. (In fact, if all laser spectra would have the same relative shape, any linear metric—even FWHM—should be as good as any other.)

In view of the importance of the spectrum tails, we also would put forward E99 as a possible metric, because it seems (at least for the spectra we considered) to be close to the ~2E95 wavelength influence range that came out of our simulation work. Although the E99 metric would also be more sensitive to measurement noise in the tails of the spectra than E95, it is much easier to determine from a measured spectrum than M_2.

Our simulations incorporate a limitation in the sense that we assumed that the spectrum-tail intensity truly goes to zero within a distance from the spectrum peak that is no larger than a few times E95, an assumption that is not easy to validate. Looking into the possible impact of such a broad, very low, but nonzero intensity background[2] [e.g., due to amplified spontaneous emission (ASE)] is therefore a topic for further investigation.

In the final section of this paper, we applied the estimators we developed to estimate bandwidth-induced OPE effects in practical cases and considered the trade-off between mean E95 and E95 stability for current systems. We showed that the proper way to ensure OPE stability (between different systems or over time for a given system) is to place an upper limit on $E95_{av} \times \Delta E95$ (i.e., the average value of E95 times the range of E95 variability). Defining an upper-limit only for E95 (as is currently being done) does not guarantee sufficient OPE control. Our conclusion, therefore, is that a tighter control on the E95-distribution and/or the possibility to tune E95 values to match scanners to each other will become necessary to avoid unacceptable OPE differences. Future laser generations will, in fact, offer both better E95 control and E95 tuning.

6 Appendix

We will now derive the approximate formula for the bandwidth contribution to the optical proximity, which will lead to Eq. (9). This derivation is not an exact proof; it is based on a number of assumptions and also uses some of the knowledge that was derived from simulations.

Our derivation is based on a threshold-on-resist-image approach for L/S imaging, and its main assumption is that we can write the image-in-resist intensity for the monochromatic case in the intensity range close to the threshold value as

$$I(x;F) \approx A_0 + A(F) + [B_0 + B(F)]x^2$$

$$\text{with} \quad A(F=0) = 0 \tag{15}$$

$$B(F=0) = 0,$$

where x is a spatial coordinate that runs perpendicular to the line that is being imaged, with $x=0$ being the position of the line center. Equation (15) then says that we assume the image intensity to vary quadratically with x around the line center, an assumption that is found to be quite accurate in case of the L/S structures considered in this paper.

$A(F)$ and $B(F)$ are functions that describe the focus dependency of the resist image. Next, we assume that the resist image is symmetric around $F=0$, which would normally be the case in the absence of lens aberrations, reticle asymmetries, etc. This symmetry assumption implies that the odd derivatives of $A(F)$ and $B(F)$ will be zero at $F=0$, which we can write as

$$A_n \equiv \frac{1}{n!}\frac{d^n A}{dF^n}(F=0) = 0, \quad \text{if } n = \text{odd number}$$

$$B_n \equiv \frac{1}{n!}\frac{d^n B}{dF^n}(F=0) = 0, \quad \text{if } n = \text{odd number}. \tag{16}$$

Consequently, we can expand $A(F)$ and $B(F)$ as

$$A(F) = A_2F^2 + A_4F^4 + A_6F^6 + \cdots$$

$$B(F) = B_2F^2 + B_4F^4 + B_6F^6 + \cdots \tag{17}$$

If we consider the resist images for the cases we have simulated in this paper (see Table 3), then we find that within a defocus range that corresponds to $\pm 2E95$, retaining the terms up to the fourth power of F in Eq. (17) fits the actually simulated resist images quite well.

Combining Eq. (2) with (15) and (17) leads to the following equation for the finite-bandwidth resist image, $I_S(x,F)$:

$$I_S(x,F) = A_0 + A_S(F) + [B_0 + B_S(F)]x^2$$

$$\text{with} \quad A_S(F) \equiv \frac{\int d\lambda S(\lambda) A(F + \lambda F_\lambda)}{\int d\lambda S(\lambda)} = A_2F_\lambda^2 M_2 + A_4F_\lambda^4 M_4 + A_6F_\lambda^6 M_6 + \cdots \tag{18}$$

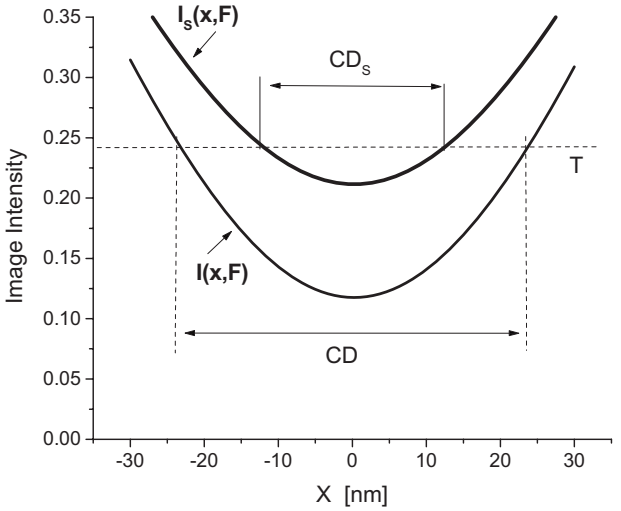

Fig. 17 Application of a fixed threshold value, T, to deduce CD from the resist images of the monochromatic (I) and finite-bandwidth (I_S) cases.

$$B_S(F) \equiv \frac{\int d\lambda S(\lambda) B(F + \lambda F_\lambda)}{\int d\lambda S(\lambda)} = B_2F_\lambda^2 M_2 + B_4F_\lambda^4 M_4 + B_6F_\lambda^6 M_6 + \cdots$$

M_2, M_4, and M_6 are the second, fourth and sixth moment of the laser spectrum S, defined as

$$M_n(S) \equiv \frac{\int d\lambda S(\lambda)\lambda^n}{\int d\lambda S(\lambda)}. \tag{19}$$

To obtain the monochromatic and finite-bandwidth CD values, which we will write as $\mathrm{CD}(F)$ and $\mathrm{CD}_S(F)$, respectively, we must apply a (constant) intensity threshold T to the image intensities described by Eqs. (15) and (18), as illustrated in Fig. 17:

$$I(x = CD(F)/2, F) = T = I_S(x = \mathrm{CD}_S(F)/2, F). \tag{20}$$

Equation (20) can then be transformed into an equation for the bandwidth-induced CD change, i.e., $\Delta\mathrm{CD}_S \approx \mathrm{CD}_S - \mathrm{CD}$. If we evaluate this CD difference at $F=0$, and retain only terms that are linear in $\Delta\mathrm{CD}_S$, Eq. (20) can be transformed into

$$\Delta\mathrm{CD}_S(F=0) = -\frac{2}{\mathrm{CD}_0}\frac{A_S(0) + B_S(0)(\mathrm{CD}_0/2)^2}{B_0 + B_S(0)}, \tag{21}$$

where $\mathrm{CD}_0 \approx \mathrm{CD}(F=0)$.

Both from the simulations as well as from the experiments of this paper, we would expect $\Delta\mathrm{CD}_S$ to be proportional to Q_F; thus, we now need to find an expression of Q_F in terms of the functions $A(F)$ and $B(F)$. This can be easily done as follows. From the simulations we know that Q_F is

not really affected by the finite bandwidth; thus, we can calculate it for the monochromatic case. The first part of Eq. (20) can then be combined with Eq. (15), leading to the following expression for $CD_S(F)$:

$$\left(\frac{\mathrm{CD}(F)}{2}\right)^2 = \frac{T - A_0 - A(F)}{B_0 + B(F)}. \tag{22}$$

Equation (22) can now be used to calculate the derivatives $d^n\mathrm{CD}/dF^n$ at $F=0$. Taking the first derivative of Eq. (22), for example, leads to

$$\frac{d\mathrm{CD}(F)}{dF} = -\frac{2}{\mathrm{CD}(F)[B_0 + B(F)]}\left[\frac{dA(F)}{dF} + \frac{dB(F)}{dF}\left(\frac{CD(F)}{2}\right)^2\right], \tag{23}$$

which can then be used to calculate the higher-order derivatives. We find that the values of these derivatives are nonzero only for even values of n (which is a direct consequence of the focus-symmetry assumption of Eq. (16), and that the even-order derivatives can be written as

$$Q_F^{(n)} \equiv \frac{1}{n!}\frac{d^n\mathrm{CD}}{dF^n}(F=0) = -\frac{2}{\mathrm{CD}_0 B_0}\left[A_n + B_n\left(\frac{\mathrm{CD}_0}{2}\right)^2\right] \quad \text{for } n = 2,4,6,\ldots \tag{24}$$

(Note that we usually write Q_F instead of $Q_F^{(2)}$.)

Comparing this result to Eq. (21), we finally obtain

$$\Delta\mathrm{CD}_S(F=0) = \frac{F_\lambda^2 M_2 Q_F + F_\lambda^4 M_4 Q_F^{(4)} + \cdots}{1 + (B_2/B_0)F_\lambda^2 M_2 + (B_4/B_0)F_\lambda^4 M_4 + \cdots}. \tag{25}$$

In order to see whether we can further simplify Eq. (25), i.e., whether we can neglect some of the higher-order terms in the numerator and/or in the denominator, we will now make an estimate of the maximum values of these higher-order terms. To do this, we resimulated the through-focus resist images for many of the L/S and illumination-mode cases of Table 3, but now taking a very fine focus step (of ~2.5 nm) to allow a more accurate calculation of the structure-dependent parameters, B_0, B_2, and B_4.

We also need values for M_2 and M_4. To avoid divergence of the integrals (due to the experimental noise in the tails of the spectra), we now replace the measured tails by a fitted function (fitted to the tail only). This smoothes the experimental noise and facilitates the calculation of the second and fourth moment of the spectrum. Somewhat arbitrarily, we choose to retain the measured spectral data for intensities >1% of the peak value and replace the measured intensities <1% of the peak value by a fitted function. (Interesting to note is that the width of the interval for which the spectral intensity >1% of the peak value is quite comparable with E99.) Again arbitrarily we used a modified-Lorentz function to do the fit of the tail. Table 5 shows the values of M_2 and M_4 we then obtain, as well as the value of the shape factor η we obtained from the fit of the spectrum tail. (Note that the M_2 values we now obtain are very close to the 29-points value of Table 2.)

Table 5 Different metrics of our laser spectra, now obtained after replacing the measured tails by a fit with a Modified–Lorentz function.

Spectrum Label	E95 (pm)	E99 (pm)	M_2 (pm^2)	M_4 (pm^4)	η
*S*0	0.27	0.468	0.0048	1.74×10^{-4}	4.1
*S*1	0.233	0.360	0.00355	0.69×10^{-4}	8.2
*S*2	0.378	0.593	0.0079	3.5×10^{-4}	4.7
*S*3	0.160	0.224	0.0016	0.11×10^{-4}	5.7
*S*4	0.218	0.285	0.0036	0.51×10^{-4}	3.5
*S*5	0.327	0.522	0.0055	2.5×10^{-4}	4.7
*S*6	0.214	0.312	0.00291	0.40×10^{-4}	5.9

Combining the calculated B_0 and B_4 data with the values of M_2 and M_4 of Table 4, and reminding that $F_\lambda < 0.5\ \mu\mathrm{m/pm}$, we find that, in all cases considered, $|(B_4/B_0)F_\lambda^4 M_4| < \sim 0.01$. This implies that Eq. (25) can, without any real loss of accuracy, be simplified to

$$\Delta\mathrm{CD}_S(F=0) \approx \frac{F_\lambda^2 M_2 Q_F + F_\lambda^4 M_4 Q_F^{(4)}}{1 + (B_2/B_0)F_\lambda^2 M_2}, \tag{26}$$

i.e., the fourth-order terms in Eq. (25) can be left out.

A numerical evaluation of the terms $(B_2/B_0)F_\lambda^2 M_2$ and $F_\lambda^2 M_2 Q_F^{(4)}$ for the cases we simulated, shows that these are not necessarily negligible, but can modify the $\Delta\mathrm{CD}_S$ prediction by up to ~10%. Thus, leaving them out, i.e., further simplifying Eq. (26) to

$$\Delta\mathrm{CD}_S(F=0) \approx F_\lambda^2 M_2 Q_F \tag{27}$$

introduces some error. We tried to estimate the error by calculating $\Delta\mathrm{CD}_S$ using Eqs. (20) and (21) and then fitting this data using Eq. (7), as we did before, so that we can compare the fitted slope-coefficient, m_2^{fit}, to M_2 as calculated from the spectrum. Compiling all results, we arrive at the correlation result shown in Fig. 18. The correlation factors we obtain are between 0.93 and 0.99, suggesting that the simplification of Eq. (27) introduces an error up to ~7% for the cases simulated here.

The reason why the correlation slope in Fig. 18 is closer to 1 than in Fig. 9 is that we have calculated Q_F in a different, more accurate, way than we did earlier. We introduced this factor in Eq. (5), in which we model the CD(F) curves by a simple parabola. Careful examination of the simulated threshold-on-resist-image CD(F) data, which we are using in this Appendix, however, reveals that this threshold CD data is represented better by the following, extended equation:

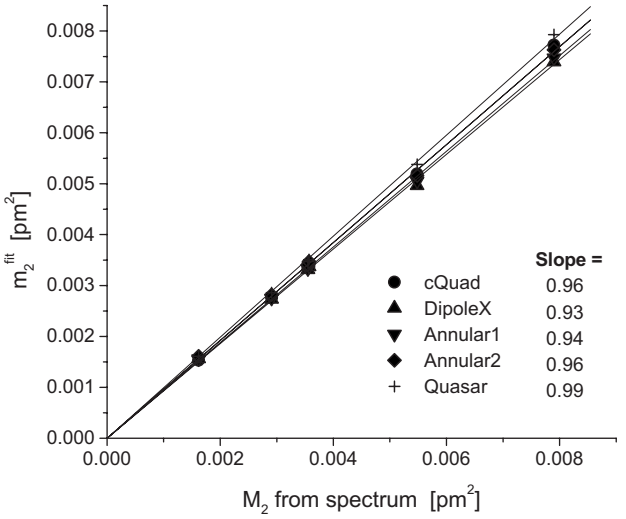

Fig. 18 Correlation of m_2^{fit} to M_2 as calculated from the laser spectrum. We determined Q_F from the six-order CD(F) polynomial fit of Eq. (28).

$$\text{CD}(F) = \text{CD}_0 + Q_F(F-F_0)^2 + Q_F^{(4)}(F-F_0)^4 + Q_F^{(6)}(F-F_0)^6 \tag{28}$$

(where $F_0=0$ in case of a threshold-on-resist-image approach). The introduction of a fourth- and sixth-order term not only fits the data better, but also changes the value of Q_F and hence of m_2^{fit}. This, in turn, improves the correlation between m_2^{fit} and M_2, as Fig. 18 clearly shows. Thus, ironically, we seem to need more F-sampling points to reliably calculate Q_F than we need to accurately calculate ΔCD_S. Of course, in a practical case, where we usually do not know the exact shape of $S(\lambda)$ in the first place and therefore can only make estimates of the bandwidth effect, there is also no need for highly accurate values of Q_F, and therefore, Eq. (5) would be adequate.

Acknowledgments

Many of the simulations of this study were done by Giuseppe Citarella and Andreas Erdmann of the IISB Fraunhofer Institute in Erlangen, Germany (under the IMEC-IISB 2005-2007 contract), using their in-house lithography simulator DrLitho©. Jeroen Van de Kerkhove (IMEC) very skillfully did most of the experimental work. We acknowledge Nigel Farrar, Rob Rafac, Vladi Gerginov, Henk Bos, and Emile Merkus from Cymer and Charles Schaap from ASML for valuable discussions and for actively supporting this bandwidth-related work in our imperfection-sensitivity study, in general. We also had useful discussions with Aksel Goehnermeier and Vladan Blahnik (Zeiss) and Sara Loi (ST Microlelectronics).

References

1. A. Kroyan, J. Bendik, O. Semprez, N. Farrar, C. Rowan, and C. Mack, "Modeling the effects of excimer laser bandwidths on lithographic performance," *Proc. SPIE* **4000**, 658–664 (2000).
2. A. Kroyan, I. Lalovic, and N. Farrar, "Effects of 95% intergral vs. FWHM bandwidth specifications on lithographic imaging," *Proc. SPIE* **4346**, 1244-1253 (2001).
3. A. Kroyan, I. Lalovic, and N. Farrar, "Contribution of polychromatic illumination to optical proximity effects in the context of deep-UV lithography," *Proc. SPIE* **4562**, 1112 (2002).
4. K. Lai, B. Fair, C. Progler, D. Ames, I. Lalovic, A. Kroyan, N. Farrar, K. Ahmed, "Chromatic aberration impacts on 0.68NA KrF lithographic imaging," *Contribution to the Arch Interface Microlithography Symp.* (2001).
5. K. Lai, I. Lalovic, B. Fair, A. Kroyan, C. Progler, N. Farrar, D. Ames, and K. Ahmed, "Understanding chromatic aberration impacts on lithographic imaging," *JM3*, **2**, 105-111 (2003).
6. T. Brunner, D. Corliss, S. Butt, T. Wiltshire, C. P. Ausschnitt, and M. Smith, "Laser bandwidth and other sources of focus blur in lithography," *Proc. SPIE* **6154**, 61540V-1-8 (2006).
7. K. Huggins, T. Tsuyoshi, M. Ong, R. Rafac, C. Treadway, D. Choudhary, T. Kudo, S. Hirukawa, S. Renwick, and N. Farrar, "Effects of laser bandwidth on OPE in a modern on lithographic tool," *Proc. SPIE* **6154**, 61540Z-1-12 (2006).
8. I. Lalovic, O. Kritsun, J. Bendik, M. Smith, C. Sallee, and N. Farrar, "Fast and accurate laser bandwidth modeling of optical proximity effects," *Proc. SPIE* **6730**, 67301X-1-14 (2007).
9. We try to avoid the more traditional but confusing term "aerial-images" intensity. What we mean with "resist-image" intensity is the image intensity in the resist, just below the resist surface.
10. Commercial simulators, such as PROLITH™ (as of version 9.3.1), now allow the user to directly input the F_λ value and a corresponding laser spectrum file, generated from laser spectrometry data, which is accessible to the laser manufacturer.
11. I. Lalovic, N. Farrar, K. Takahashi, E. Kent, D. Colon, G. Rylov, A. Acheta, K. Toyoda, and H. Levinson, "RELAX: Resolution Enhancement by laser-spectrum adjusted exposure," *Proc. SPIE* **5754**, 447–455 (2005).
12. We used Eq. (856.08) from *Tables of Integrals and Other Mathematical Data*, H. B. Dwight, 4th edition, 1972, Macmillan.
13. See, e.g., ⟨http://en.wikipedia.org/wiki/Linear_regression⟩

Peter De Bisschop received his PhD in physics from the University of Leuven (Belgium) in 1984 and started working at IMEC in 1986. In 1995, he joined the Optical Lithography department, where he has done research in several optical-imaging-related fields, including lens aberrations, impact of illumination-source shape, hard pellicles, stray light, optical proximity, and metrology.

Ivan Lalovic has worked in research, development, and manufacturing of lithographically patterned semiconductor devices. He started his career at Hewlett Packard and has consequently held various engineering and management roles at Cymer, Inc., and Advanced Micro Devices. He is presently the director of applications for the U.S. and Europe at Cymer. Lalovic holds a BA degree in physics from Whitman College and MSEE from the University of Washington. He has authored over 25 papers in the area of lithography imaging, semiconductor processing, and photomask technology, and holds 10 U.S. patents.

Fedor Trintchouk has contributed to the system integration of several generations of Cymer DUV light sources. Prior to joining Cymer, he worked on laser-aided plasma diagnostics, such as LIF imaging, studies of magnetic reconnection in plasmas, and EUV laser sources. Trintchouk holds an MS in physics from Moscow Institute of Physics and Technology and a PhD in plasma physics from Princeton University.